

Enabling Unsupervised Discovery in Astronomical Images through Self-Supervised Representations

Koketso Mohale,¹★ Michelle Lochner,^{1,2}

¹*Department of Physics and Astronomy, University of the Western Cape, Bellville, Cape Town, 7535, South Africa*

²*South African Radio Astronomy Observatory, 2 Fir Street, Black River Park, Observatory, 7925, South Africa*

Accepted XXX. Received YYY; in original form ZZZ

ABSTRACT

Unsupervised learning, a branch of machine learning that can operate on unlabelled data, has proven to be a powerful tool for data exploration and discovery in astronomy. As large surveys and new telescopes drive a rapid increase in data size and richness, these techniques offer the promise of discovering new classes of objects and of efficient sorting of data into similar types. However, unsupervised learning techniques generally require feature extraction to derive simple but informative representations of images. In this paper, we explore the use of self-supervised deep learning as a method of automated representation learning. We apply the algorithm Bootstrap Your Own Latent (BYOL) to Galaxy Zoo DECaLS images to obtain a lower dimensional representation of each galaxy. We briefly validate these features using a small supervised classification problem. We then move on to apply an automated clustering algorithm, demonstrating that this fully unsupervised approach is able to successfully group together galaxies with similar morphology. The same features prove useful for anomaly detection, where we use the framework ASTRONOMALY to search for merger candidates. Finally, we explore the versatility of this technique by applying the exact same approach to a small radio galaxy dataset. This work aims to demonstrate that applying deep representation learning is key to unlocking the potential of unsupervised discovery in future datasets from telescopes such as the Vera C. Rubin Observatory and the Square Kilometre Array.

Key words: methods: data analysis – surveys – galaxies: general

1 INTRODUCTION

Rapid advancements in astronomical surveys have resulted in the production of volumes of data too large for human experts to manually inspect. Projects such as Galaxy Zoo (Lintott et al. 2008) employ the use of citizen scientists to label galaxy morphology at large scales. Examples of applications of these morphology classifications include studies of the host galaxies of active galactic nuclei (Schawinski et al. 2009), investigations of merging galaxies (Darg et al. 2010), and the formation of bars in spiral galaxies (Simmons et al. 2014). However, these classifications are limited in that they require hand-labelled data and the rapid increase of data volumes means that eventually even citizen science projects will not be able to keep up. Additionally, citizen scientists may not necessarily have the training required to make more nuanced classifications or identify particularly anomalous sources.

Unsupervised machine learning has the potential to leverage large unlabelled datasets, allowing for data-driven discovery and exploration. These algorithms can also be used to create training sets for downstream supervised applications far more quickly than random labelling. There have been numerous applications of unsupervised learning in astronomy, including the application of clustering and anomaly detection to radio galaxies (Ralph et al. 2019; Gupta et al.

2022), the detection of anomalous spectra in LAMOST data (Yang et al. 2023) and the hunt for rare transients and variables in Deeper Wider Faster optical data (Webb et al. 2020). Lochner & Bassett (2021) introduced the general-purpose anomaly detection framework ASTRONOMALY, which was later applied to data from the MeerKAT telescope to discover a highly unusual radio source (Lochner et al. 2023).

There is also a long history of applying unsupervised techniques to achieve automatic clustering of optical galaxies into similar morphology, which include early applications of artificial neural networks to photometric galaxy parameters (e.g. Lahav et al. 1996; Naim et al. 1997; d’Abrusco et al. 2007). The motivation behind these efforts is not simply to automate otherwise tedious tasks, but also to allow the possibility of discovering new classes of objects or a more physically motivated categorisation of galaxies.

However, unsupervised algorithms usually cannot work directly with high dimensional data such as images (with the notable exception of the rotation-invariant self-organising maps of Polsterer et al. 2019) and instead require lower dimensional representations called features. In the case of galaxy morphologies, these features could include photometric colours or shape parameters such as the Gini coefficient. The choice of feature extraction method will generally dictate the success of the machine learning algorithm.

Deep learning algorithms (e.g. LeCun et al. 2015), particularly convolutional neural networks (CNNs), have revolutionised the field

★ E-mail: koketso.kjay@gmail.com

of image recognition due to their ability to obtain meaningful representations from images without requiring explicit feature selection. This has led to their use as general-purpose feature extractors, as was demonstrated in Walmsley et al. (2022) where a pretrained convolutional neural network dramatically outperformed simpler, hand-designed morphological features for unsupervised tasks on the optical dataset Galaxy Zoo DECaLS (Walmsley et al. 2020a). Etsebeth et al. (2023) recently demonstrated the same features could be used for highly effective anomaly detection among nearly 4 million galaxies in the larger DECaLS dataset (Dey et al. 2019).

The downside of using a pretrained network as a feature extractor is that it requires the data be relatively similar to the dataset it was originally trained on in order to obtain the best performance. It also requires a large, labelled dataset for training which does not exist for many fields, such as high resolution radio astronomy. In a recent paper, Vafaei Sadr et al. (2022) applied a CNN to the Galaxy Zoo DECaLS dataset, repeatedly retraining the network with human-provided labels to improve the features learned in order to quickly detect interesting anomalies. While this approach is very promising, it would require somewhat expensive retraining of the CNN with each iteration which may not be possible in all scenarios.

Self-supervised learning offers a promising alternative. Modern approaches to unsupervised clustering of galaxy images tend to rely on autoencoders to learn a representative feature space (for example, Spindler et al. 2021; Cheng et al. 2021; Zhou et al. 2022; Fielding et al. 2022). Autoencoders are trained to reproduce the input data identically and in the process, learn a lower dimensional representation of the image dataset. Newer self-supervised techniques, including contrastive and non-contrastive learning, instead apply augmentation to introduce random variations in the data and train the algorithm to recognise these pairs of augmented images as being the same. This form of self-supervised learning is gaining popularity as a method of learning effective representations without labels (Huertas-Company et al. 2023).

Contrastive learning, which includes both positive and negative augmented image pairs, has been applied several times to optical galaxy images. Hayat et al. (2021) and Stein et al. (2021, 2022) use contrastive learning for an impressive array of applications including galaxy morphology classification, photometric redshift estimation, strong lens discovery and similarity searches. Sarmiento et al. (2021) applied contrastive learning to investigate galaxy physics in integral field unit data, while Wei et al. (2022) showed that learned representations can be applied across different optical datasets.

While this recent body of work shows that contrastive learning can be a powerful tool for a myriad of applications, it can be computationally demanding. Non-contrastive learning, specifically the technique Bootstrap Your Own Latent (BYOL, Grill et al. 2020), is a more viable option when computational resources are limited. Slijepcevic et al. (2023) showed the potential of BYOL as a foundation model for radio galaxy images, which can be fine-tuned for classification tasks on new datasets.

The goal of this paper is to develop a methodology for data exploration, as an initial step for building training sets, obtaining the more obvious morphology groups and for detecting anomalies for large and unlabelled datasets. We apply self-supervised learning to two different datasets, for the purpose of learning representations that can be used for unsupervised learning tasks. As well as demonstrating the performance of these representations for a simple supervised classification task, we apply automated unsupervised clustering and anomaly detection with active learning as example downstream tasks. While the main dataset used in this paper consists of optical images

of galaxies, we also apply the same methods to a small radio galaxy dataset to demonstrate their general utility.

We start by focusing on the popular hand-labelled optical dataset Galaxy Zoo DECaLS, which we describe in Section 2. We outline our use of a pretrained network for removing artefacts in Section 3 and the methodology of using self-supervised learning to extract useful features in Section 4. We then demonstrate the effectiveness of these features in a series of different applications. We make use of supervised classification in Section 5 to demonstrate the utility of initialising the network with pretrained weights and as a baseline to ensure the self-supervised method is indeed learning representations that correspond to galaxy morphology. An unsupervised clustering approach is explored in Section 6 to attempt to group galaxies of similar morphology together without the need for labelling. We apply an anomaly detection algorithm in Section 7 to rapidly locate merger candidates. After exploring the use of self-supervised learning on optical data, we further demonstrate its remarkable flexibility by applying an essentially identical approach to a radio dataset in Section 8 with both a supervised classification and clustering application. Section 9 summarises our conclusions.

2 GALAXY ZOO DECALS DATA

The data used in this paper was originally sourced from the Dark Energy Camera Legacy Survey (DECaLS, Dey et al. 2019) DR5. The Galaxy Zoo DECaLS data (Walmsley et al. 2020a) is a catalogue of thousands of high resolution images, from DECaLS, of optical galaxies with a wide range of morphologies. This dataset is ideal for our work because it is large, from a modern telescope and fully labelled. Although we are primarily interested in unsupervised applications, the labels allow us to test the effectiveness of the algorithms considered before applying to unlabelled datasets in the future. The Galaxy Zoo¹ citizen science project asks users to identify morphological features of galaxies, deciding whether each object is smooth or featured, has spiral arms, bars, tidal tails etc. Galaxy Zoo DECaLS made use of a sophisticated decision tree, rather than assigning simple morphological labels, which simplifies the identification task by removing jargon but also allows fine-grained decision making when defining a morphological sample.

Volunteers are presented with a series of questions such as “*Is the galaxy simply smooth and rounded, with no sign of a disk?*” to which the answer could be “Smooth”, “Features or disk” or “Artefact”. The volunteer is then presented with the next question based on their initial answer and so traverses down the decision tree. The number of votes as well as the vote fraction for each question is recorded and these can be used to create labelled subsets that select for a certain morphology.

The images and labels we use can be found on Zenodo² (Walmsley et al. 2020b). We use the labels from versions 1 and 2 of Galaxy Zoo DECaLS³ rather than version 5, as we did not consider the improvements to the decision tree in version 5 to be as important for our application as simply having more labelled data to test with. The total number of images available from Zenodo was 269 760 and of those, 65 290 had labels from volunteers. We used the full image set for training our feature extractor (Section 4) and applying a clustering algorithm (Section 6.1) but restricted our analysis to the labelled data

¹ www.galaxyzoo.org

² <https://zenodo.org/record/4573248>

³ [gz_decals_volunteers_1_and_2.parquet](#)

for interpretation of the clustering results (Section 6.2) and the later anomaly detection application (Section 7).

2.1 Preprocessing

Slijepcevic et al. (2023) found that CNNs are sensitive to the apparent angular size of a source in a given image. To ensure the algorithm is focusing on physical morphological features, we preprocess each image to attempt to isolate and resize the central source. We use the standard sigma clipping transform available in the software package ASTRONOMALY⁴ to locate the central source and cut out background sources. This function works by first calculating the noise level in the image, using ASTROPY (The Astropy Collaboration et al. 2013, 2018, 2022), applying a 4σ threshold and then using an OPENCV (Bradski 2000) contour-finding algorithm to select all regions above this threshold. Because the source should always be located at the centre of the image, we could then select only the central contour in order to determine an appropriate bounding box around the source. We chose to enlarge the bounding box by a factor of two to ensure the entire source is contained.

It should be noted that the resulting bounding box was applied to the original image, not the sigma-clipped image. Sigma clipping can sometimes remove part of the source and a key advantage of deep learning is that it can easily learn to ignore the background anyway. Preliminary analysis suggested that the choice of whether or not to apply sigma clipping did not significantly impact our results, but this could change for more crowded fields from deeper surveys.

At times the contour-fitting procedure can fail and raise an error, usually due to large sources filling the field or very bright nearby sources such as stars or artefacts. In these cases we simply use the original image instead. After extracting the central source, we resize the image to 300x300 pixels.

3 FEATURE EXTRACTION WITH A PRETRAINED NETWORK

Our general approach is to make use of a CNN as a feature extractor, rather than a classifier. This can be done for a CNN that has been trained to solve a different task by ignoring the final classification layer of the network and instead using the outputs of the weights of the previous layer as features (as was done in Walmsley et al. (2022), Etsebeth et al. (2023) and several other examples). Here we describe the core architecture we use throughout this work and our initial experiment with a standard pretrained neural network before moving on to self-supervised learning.

3.1 Model architecture

CNNs are a type of neural network consisting of many layers of interconnected “neurons”. The key difference between CNNs and typical artificial neural networks is that the neurons of CNNs are kernels that perform convolutions across an image. This allows the network to, through training, learn an optimal set of filters through which to pass the image, resulting in a useful image representation for the downstream task. CNNs also consist of other types of layers, such as pooling and dropout layers, which are inserted to improve this representation by allowing filters to be applied on a hierarchy of

scales and also avoiding overfitting, which such complex algorithms are otherwise prone to.

We used the ResNet-18 model (He et al. 2016) as the CNN architecture for this work. ResNet-18 was found to have sufficient performance for a low computational cost. Guérin et al. (2021) performed an in-depth analysis of the use of CNNs as feature extractors for clustering tasks and found that the second last layer always provides the best representation of the images. In the case of a Resnet-18 this is the layer called “avgpool”, which produces 512 outputs to be used as features.

3.2 Visualisation of extracted features

It is particularly critical for this type of work to be able to visualise high dimensional feature spaces. In keeping with the current trend in the machine learning field, we make use of the technique Uniform Manifold Approximation and Projection (UMAP, McInnes et al. 2018). UMAP aims to learn a lower dimensional embedding that optimises for local structure, but still preserves global structures. These plots are especially useful for localising obvious outliers, determining where sources of particular types lie in feature space and for understanding the behaviour of the unsupervised algorithms we later applied to the features.

To implement UMAP for our features, we made use of the UMAP-LEARN⁵ software package (Sainburg et al. 2021). The UMAP algorithm has a number of hyperparameters. Throughout this work, we set the parameter “number of neighbours” to 15, which minimises the creation of artificial clusters and the parameter “minimum distance” to 0.01 to prioritise local structure and encourage the formation of genuine clusters.

3.3 Artefact removal with a pretrained network

Unfortunately, the preprocessing procedure of Section 2.1 inadvertently introduced artefacts into the data. While a more refined procedure may produce fewer artefacts, it is difficult to eliminate them entirely. Instead, we used the opportunity to test a novel approach to artefact removal. Before proceeding to the full feature extraction method described in the next section, we used a ResNet-18 already trained on the well-known machine learning dataset of terrestrial images called ImageNet (Russakovsky et al. 2014). This pretrained model is already a fairly effective feature extractor and we were able to trivially excise the most obvious artefacts from our dataset with these features. A UMAP plot is shown in Figure 1 displaying the cuts applied to excise the artefacts. We focused on the largest cluster of artefacts rather than trying to vigorously remove all artefacts. While the pretrained network was highly effective at removing these, it failed to usefully group similar galaxies together. We thus did not make use of this network, beyond the initial artefact removal, and instead moved on to a self-supervised learning technique as a feature extractor. The main dataset used in the rest of this work contains 232 041 images after preprocessing.

4 FEATURE EXTRACTION WITH SELF-SUPERVISED LEARNING

Self-supervised learning aims to learn useful representations of images without requiring training labels. A common approach to self-

⁴ <https://github.com/MichelleLochner/astromaly>

⁵ <https://umap-learn.readthedocs.io/en/latest/>

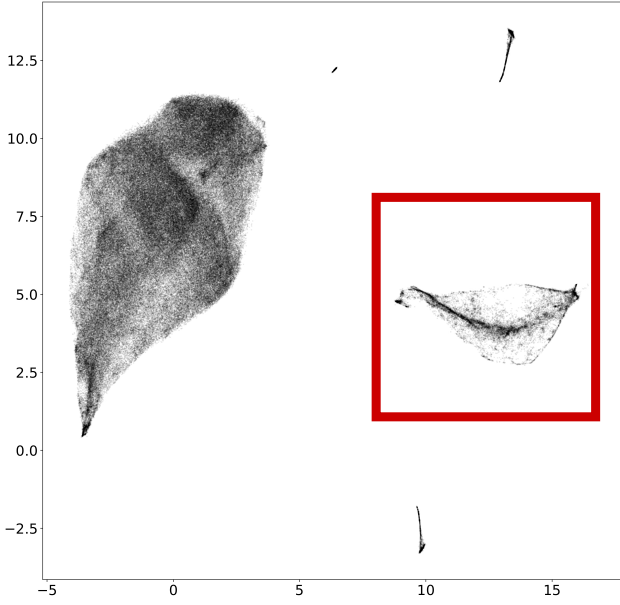


Figure 1. UMAP representation of the feature space of the whole Galaxy Zoo DECaLS data set after preprocessing, using a CNN pretrained on ImageNet as a feature extractor. The bounding box shows the selection used to remove the artefacts introduced. The x and y axes are in arbitrary units.

supervised learning is to train the model to have the same predictions for different augmentations (views) of the same image. This leads to representation collapse (e.g the model might predict the same trivial solution for all images) and self-supervised learning techniques employ different ways to circumvent this. For example, the contrastive learning algorithm SimCLR (Chen et al. 2020) uses a repulsive term, generated from negative pairs, in the loss function to prevent collapse. However, this algorithm can be resource-intensive precluding its use for this work.

Bootstrap Your Own Latent (BYOL, Grill et al. 2020), on the other hand, is a non-contrastive self-supervised learning method that requires relatively low computational resources and, somewhat surprisingly, manages to avoid representation collapse without the need for negative pairs (see Tian et al. (2021) for some recent insights and possible explanations). BYOL uses two neural networks of the same architecture, called online and target networks. In each training step they are provided with different augmentations of the same images and the target network outputs regression targets for the online network. The weights of target network (ξ) are an exponential moving average of the online network weights (θ) and are updated according to equation Equation 1. Here $\tau \in [0, 1]$ is a target decay parameter.

$$\xi_i \leftarrow \tau \xi_{i-1} + (1 - \tau) \theta \quad (1)$$

By training on a large dataset with random augmentations, this pair of interacting networks is able to produce a representation of the images that reliably groups similar objects together without the need for labels.

Hyperparameter	Value
Network architecture	Resnet-18
Epochs	20
Optimiser	Adam
Learning rate	0.0001
Batch size	128
τ	0.99
Neurons in projection layer	100

Table 1. Hyperparameter values used for training the BYOL algorithm.

4.1 Augmentations and hyperparameters

We use the package BYOL-PYTORCH⁶ (Chen & He 2020) to apply the BYOL algorithm. The hyperparameters we selected are shown in Table 1. We fix the number of epochs to 20, which we found to be computationally efficient while still being sufficient to produce excellent representations. Further training did not improve our results. We chose not to use a separate validation set to maximise the number of sources available for training, instead relying on the downstream supervised learning application to assess the features (see Section 5).

The effectiveness of BYOL is heavily dependant on the augmentations. Grill et al. (2020) includes recommended augmentations to use for terrestrial dataset. We find that, just as in the case of radio data (Slijepcevic et al. 2023), augmentations have to be adjusted to be suitable for the optical datasets. Preprocessing and augmentations affect the representations that BYOL will learn and it is important that the variance in the background of galaxies does not dominate the variances in different morphology types.

We use the augmentations gaussian blurring, vertical flip, horizontal flip each with probability 0.5. We apply the augmentation resized crop with the smallest value for cropping the image set to 0.7, rotations by random angles $\theta \in [0 - 360]$, setting the probability of applying either to 0.7.

In terms of computational requirements, we use a single NVIDIA P100, 16-core GPU (with 116GB of RAM) and find that BYOL trains in approximately 11 hours.

4.2 Dimensionality reduction

Most unsupervised learning algorithms do not scale well to high dimensional spaces. For this reason, we further reduced the dimensionality of the features using Principal Component Analysis (PCA, Pearson 1901; Hotelling 1933).

It is natural to consider using the reduced features derived from a manifold learning algorithm such as t-SNE (van der Maaten & Hinton 2008) or UMAP (McInnes et al. 2018) instead of PCA, since these algorithms are non-linear and more flexible. However, we found that PCA preserves *global* structure better than manifold learning approaches and it is precisely the linearity of PCA that reduces the risk of creating artificial clusters in feature space (which manifold learning can sometimes produce). We thus elected to use PCA to reduce dimensionality for downstream tasks and UMAP purely for visualisation purposes.

We applied PCA to the deep representations, as obtained from the hidden layer “avgpool”, keeping 95% of the variance and thus reducing to 29 principal components. We exclusively used the reduced feature space for clustering and anomaly detection.

⁶ <https://github.com/lucidrains/byol-pytorch>

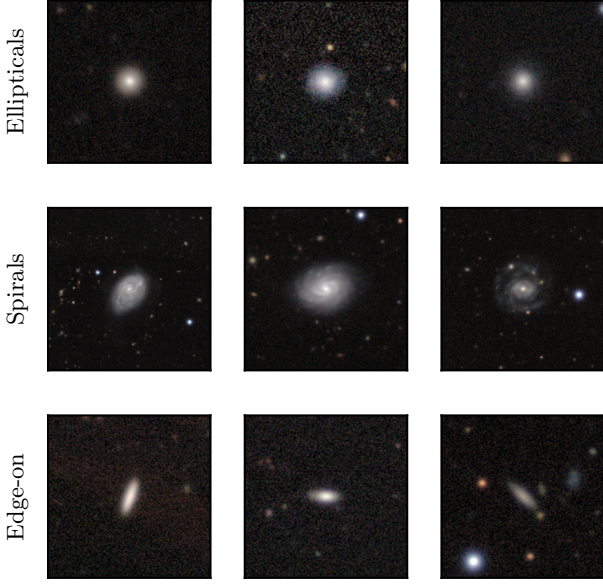


Figure 2. Examples of each class in the evaluation set representing ellipticals (top row), spirals (middle row) and edge-on galaxies (bottom row).

5 EVALUATION OF EXTRACTED FEATURES

5.1 Evaluation subset

It is challenging to evaluate the performance of a self-supervised learning algorithm since they are designed to operate without any labels by definition. The standard approach is usually to evaluate the extracted features in a downstream task. We thus opted to use our features to solve a simple, if contrived, supervised classification problem as an initial test of performance.

We selected a small sample of sources that should be considered relatively easy to classify: round ellipticals, spiral galaxies and edge-on galaxies. Because Galaxy Zoo makes use of a decision tree rather than hard morphological classifications, cuts must be used to extract a confident sample of sources, which we describe below. In every case, we ensured a minimum number of five votes for the question being considered (the same threshold used in Domínguez Sánchez et al. (2018)). We also selected only galaxies most likely not to host a merger, by requiring `merging_merger_fraction` < 0.2. The number of each class that meets the cuts is given in brackets.

- Round ellipticals (4231):
`smooth-or-featured_smooth_fraction` > 0.8 and
`how-rounded_completely_fraction` > 0.8.
- Spirals (4034):
`smooth-or-featured_featured-or-disk_fraction` > 0.8 and
`has-spiral-arms_yes_fraction` > 0.8.
- Edge-on galaxies (5344):
`disk-edge-on_yes_fraction` > 0.8.

Figure 2 shows three randomly chosen examples for each of the classes.

To evaluate the utility of our extracted features for this three-class classification problem, we applied a simple k-nearest neighbours (KNN) algorithm (Fix & Hodges 1951; Cover & Hart 1967). For this problem, we found that KNN performed just as well on the original

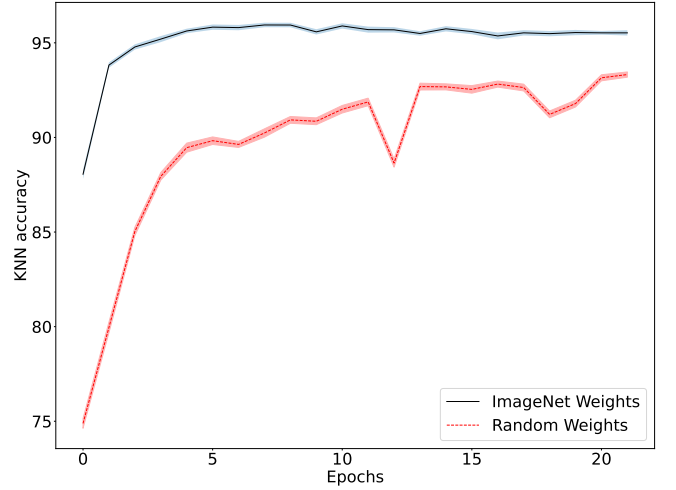


Figure 3. Accuracy of a KNN algorithm applied to the Galaxy Zoo DECaLS evaluation subset as a function of epoch. We use the features derived from training BYOL on the galaxy images and compare initialising the weights randomly with initialising them from a network pretrained on ImageNet. For each epoch, the accuracy is computed for 50 iterations of training-test splits with the mean represented as a line and the standard deviation as an envelope. Fine-tuning increases the accuracy and convergence speed for this dataset.

feature space as on the PCA-reduced space. Thus, all reported results using KNN are applied in the original 512-dimensional space.

The SCIKIT-LEARN (Pedregosa et al. 2011) implementation of KNN was used and we set the number of neighbours to 5 and the distance metric to Minkowski. We selected the overall accuracy as an easily-interpretable metric, given that the classes are approximately balanced. As our focus is not on supervised learning and we simply use this as a tool to evaluate our features, we did not further optimise the classifier. In all cases, the KNN algorithm was trained on a randomly chosen 75% of the evaluation subset and the accuracy was computed on the remaining 25%. For each epoch we run KNN 50 times with a new random training-test split for each iteration and investigate the mean and standard deviation to ensure the algorithm converges to a roughly constant accuracy.

While the accuracy is a useful tool to monitor the performance of the BYOL algorithm as a function of epoch, it's important to note that the algorithm is still trained in a completely self-supervised way and that this accuracy information is never fed back to the network.

5.2 Comparing transfer learning and random weight initialisation

It is most common to train a self-supervised learning algorithm with the weights initialised to random values. However, inspired by the performance of the pretrained network in Walmsley et al. (2022) and many other examples of fine-tuning, we decided to compare the performance of BYOL initialised with random weights with that of ImageNet-initialised weights. We thus essentially use BYOL as a method of fine-tuning the network described in Section 3.3 to adapt the network to our particular dataset.

Figure 3 shows the accuracy of KNN applied to the evaluation set when training a model initialised with ImageNet weights against one with randomised initial weights. The results show that not only do the fine-tuned BYOL features start with a 13% higher accuracy, the network also converges quicker to a relevant feature space and has

a higher peak accuracy after 20 epochs. While the accuracy of the random-start network may eventually be comparable to that of the fine-tuned network, fine-tuning provides significant gains in terms of reducing computational requirements. While we use the accuracy purely as a comparison metric between the two approaches, it is also worth noting that 95% accuracy is excellent performance and shows the representation produced by BYOL is useful for downstream tasks. Having evaluated its performance, for the remainder of this work we use the features derived from applying BYOL, initialised with the ImageNet weights, to the entire Galaxy Zoo DECaLS dataset after preprocessing.

6 CLUSTERING

After extracting features, evaluating their performance on a small supervised learning problem and reducing their dimensionality with PCA, we next turned our attention to the main goal of this paper: to automatically cluster similar objects together in an unsupervised manner.

6.1 Bayesian Gaussian mixture model

We chose to apply a Bayesian Gaussian mixture model (BGMM, [Attias 1999](#)) for this problem. The aim of this clustering approach is to approximate the data as a mixture of Gaussian distributions, each with a mean, covariance and overall weight. These Gaussians then form the clusters. A BGMM specifically applies Bayesian inference to learn the parameters of these Gaussians.

We use the `BAYESIANGAUSSIANMIXTURE` library from `SCIKIT-LEARN` ([Pedregosa et al. 2011](#)). We ran BGMM with the number of components set to 20. The intuition behind the number is based on the number of density regions we observed on the UMAP feature space. However, we note that the BGMM implementation is able to set the weights of individual Gaussians very low making the input number of components an upper limit in reality. We set the weight concentration prior to 0.5 to force BGMM to focus more on global structure, and ran 10 initialisations with the maximum number of iterations set to 1000.

We applied the clustering algorithm to the features from the full Galaxy Zoo DECaLS dataset (after preprocessing) to obtain a total of 20 clusters labelled 0-19. BGMM is able to identify densities consistent with those that we see on the feature space in the UMAP plots. However we observe some disagreement between BGMM and UMAP since the clustering is applied directly on the principal components.

[Figure 4](#) shows examples of galaxies that correspond to several of the clusters that can be seen on the UMAP plot. Combining self-supervised with unsupervised learning does appear to successfully group together sources with similar morphologies, such as elliptical and spiral galaxies, as well as edge-on galaxies and those with a prominent bulge. [Figure 5](#) shows some more complex examples, suggesting that at times the algorithm may be picking up on non-physical properties such as a particularly “zoomed out” image or the presence of a companion. Improved preprocessing could perhaps clean up some of these clusters but blending will likely remain a difficult challenge to these algorithms as surveys increase in depth and hence source density.

[Figure 6](#) shows how the clustering algorithm effectively selects artefacts, missed by the approach presented in [Section 3.3](#). This suggests that unsupervised techniques could provide a relatively

lightweight method of detecting and removing artefacts that may be otherwise missed by automated pipelines.

6.2 Cluster analysis with volunteer labels

While it is visually apparent that the clustering algorithm successfully groups galaxies of similar morphology together, we can investigate this more deeply by making use of the Galaxy Zoo decision tree user labels. [Figure 7](#) highlights the distribution of vote fractions for several key questions in the Galaxy Zoo decision tree, for galaxies in each cluster, as well as for the full labelled sample for comparison. To remove spurious components of the distributions, we set a rather stringent minimum threshold of 10 votes for each question. Using these distributions, we can investigate more deeply the types of galaxy residing in each cluster.

Based on visual inspection of examples of cluster members, we excluded clusters 7, 8, 9, 11, 13, 15, 17 and 19 from the plots as they predominantly contained artefacts (some examples of these are shown in [Figure 6](#)). Inevitably, some clusters (most notably cluster 19) contain some real and interesting sources among the artefacts, but these sources are in the minority. It should be noted that most of the artefacts in these clusters were introduced during preprocessing and were not present in the original data. While the preprocessing could certainly be improved to avoid the inclusion of these artefacts, artefacts are nonetheless often introduced in scientific pipelines and it is encouraging to see the clustering algorithm is able to trivially detect these. The number of galaxies excluded is 5332, out of a total of 65290 sources. We use the distributions of [Figure 7](#) to better understand the types of galaxies found in each of the remaining clusters.

The first Galaxy Zoo decision tree question we considered is “*Is the galaxy simply smooth and rounded, with no sign of a disk?*”. In the top panel of [Figure 7](#), we show the distributions for the fraction of votes for “Features or disk” (in other words, the galaxy is not smooth or an artefact). The distributions for clusters 1, 3, 12 and 14 strongly suggest they are largely smooth and probably elliptical galaxies. It is interesting to note that clusters 1 and 12 contain well-resolved sources while 3 and 14 are much lower resolution, which may result in the citizen scientists voting them to be smooth. Cluster 5 appears to consist almost entirely of spirals, while the remaining clusters have less clean distributions. Clusters 0 and 18 contains a mix of morphologies, but closer investigation of the question “*Is there any sign of a spiral pattern?*” (not shown in [Figure 7](#)), as well as inspection of the examples in [Figure 4](#), suggests that these groups consists largely of spirals.

Cluster 6 shows fairly broad distributions throughout, which reflects the fact that this cluster is not well localised in [Figure 5](#). Inspection of the examples of cluster members suggests that algorithm grouped together objects with nearby (usually coincident) sources, rather than primarily by morphology. Although not shown in order to reduce complexity of the figure, we also investigated the “Artefact” answer to the first question in the Galaxy Zoo decision tree. Only clusters 16 and 19 indicated a higher than average number of artefacts. We discarded cluster 19 based on visual inspection indicating that artefacts dominated this cluster. Cluster 16 however, consists of a mix of artefacts and galaxies with interesting morphology so we kept cluster 16 in the sample.

We further investigated these clusters by examining the answer to the question “*How rounded is it?*”, focusing on the “Cigar shaped” galaxies in the second panel of [Figure 7](#). As this question in the decision tree only applies to galaxies that appear smooth, we only considered objects for which the fraction of votes for a smooth object

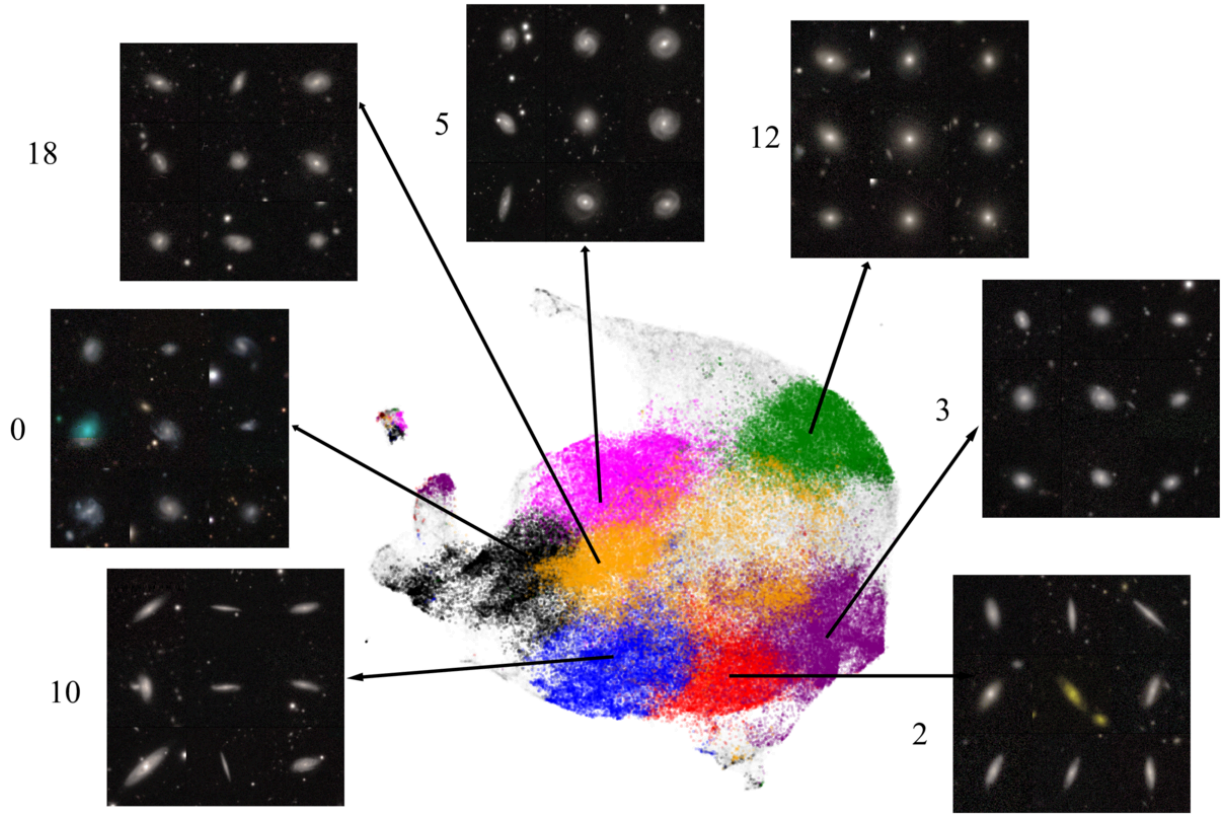


Figure 4. UMAP plot of cluster samples corresponding to morphologies that include flat disk galaxies (2 and 10), bright centered tight spirals (5 and 18), and bright centered high resolution ellipticals (12).

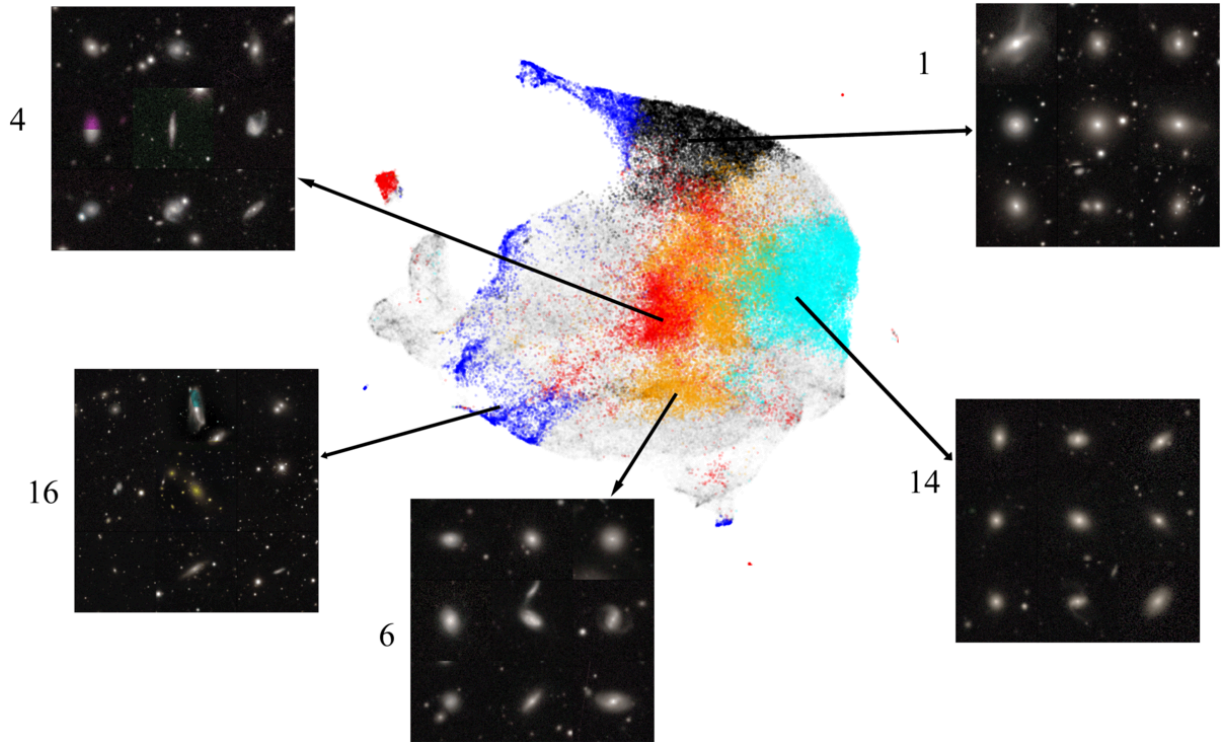


Figure 5. UMAP plot of cluster samples corresponding to morphologies that can be challenging to categorise. The feature space shows a larger disagreement between UMAP and BGMM in the case of these type of galaxies. The confusion mostly comes from heavy background noise (cluster 16, 4 and 1) as well as low resolution (cluster 14).

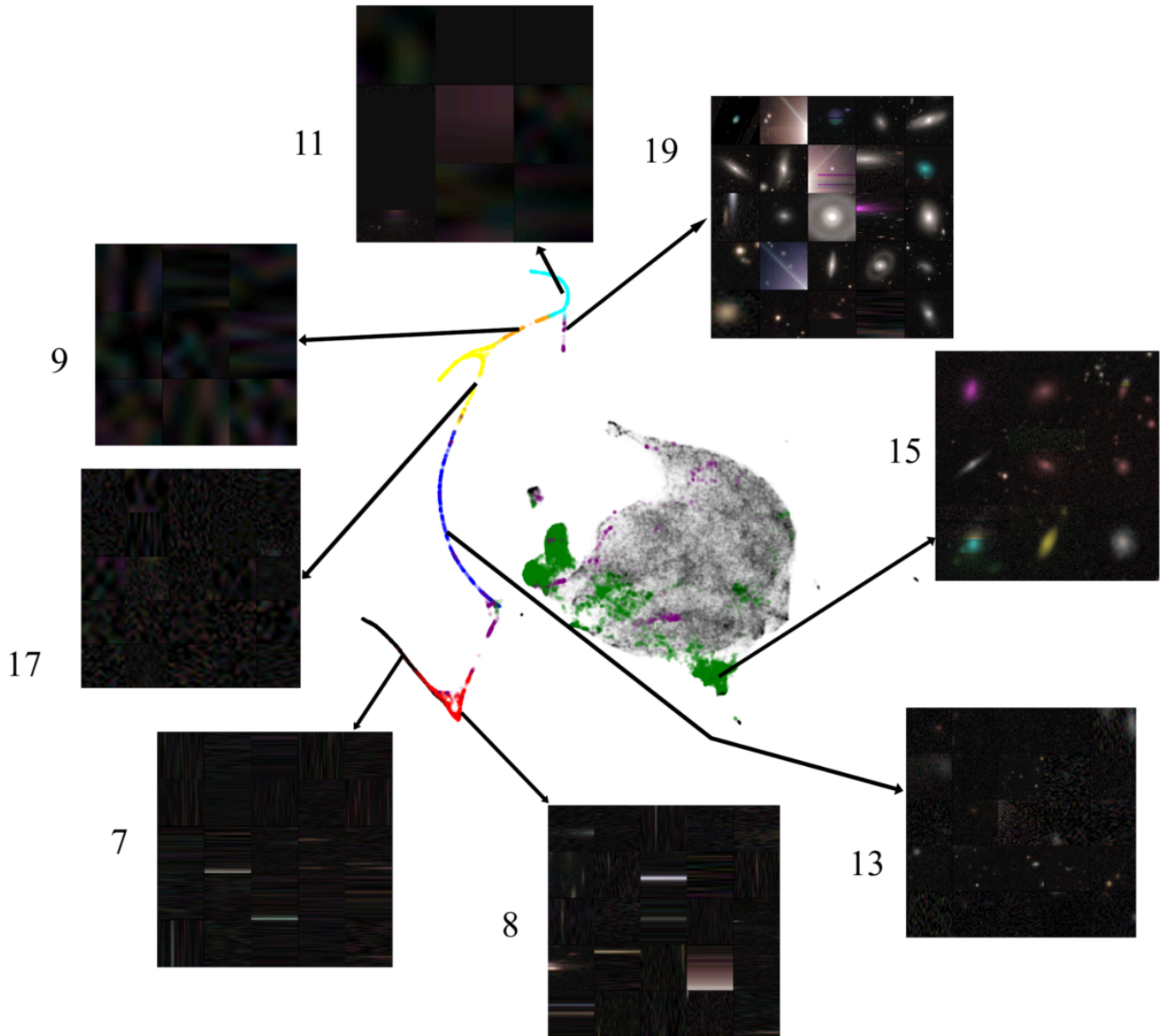


Figure 6. UMAP plot of cluster samples that correspond to artefacts. These artefacts tend to separate well from the main population and group together by type, indicating that self-supervised features are effective at identifying artefacts that may have been otherwise missed.

is greater than 0.5. We also considered the question “*Could this be a disk viewed edge-on?*” in the third panel. We applied a threshold of 0.5 to the fraction of votes that consider the galaxy to be featured. These two plots together show that clusters 2 and 10 both consist of elongated galaxies, but the algorithm is not able to easily distinguish between cigar-shaped ellipticals and edge-on spirals (although more cigar-shaped galaxies seem to occur in cluster 2 than 10). This is not surprising as edge-on spirals and elongated ellipticals can be indistinguishable even for a human if the inclination angle is high enough or the resolution low. Finally, we note that cluster 16 seems to have a mix of edge-on and face-on galaxies and is one of the more complex grouping of galaxies.

In the fourth panel of Figure 7, we considered the question “*How prominent is the central bulge, compared with the rest of the galaxy?*” and focused on the distributions for the answer “Dominant bulge”.

Similarly to the previous questions, we required the fraction of votes for the featured question to be greater than 0.5. This plot reveals that although clusters 12 and 14 consist of mostly ellipticals, they also include some disk galaxies with prominent bulges that appear similar to ellipticals. By viewing the examples in Figure 4 and Figure 5, it is easy to see how these objects can be confused even by a human. Cluster 1, which contains some mixed morphologies, also seems to consist mostly of galaxies with a dominant bulge, although we note that this cluster contains a significant number of artefacts.

The final panel of Figure 7 focuses on the question “*Is the galaxy merging or is there any sign of tidal debris?*” Because this question has multiple answers, we focused on the negative to look for sources that have any indication of mergers at all. We once again required at least 50% of users to have voted that the galaxy is featured to include it in the sample. The plot suggests that clusters 1, 4 and 16

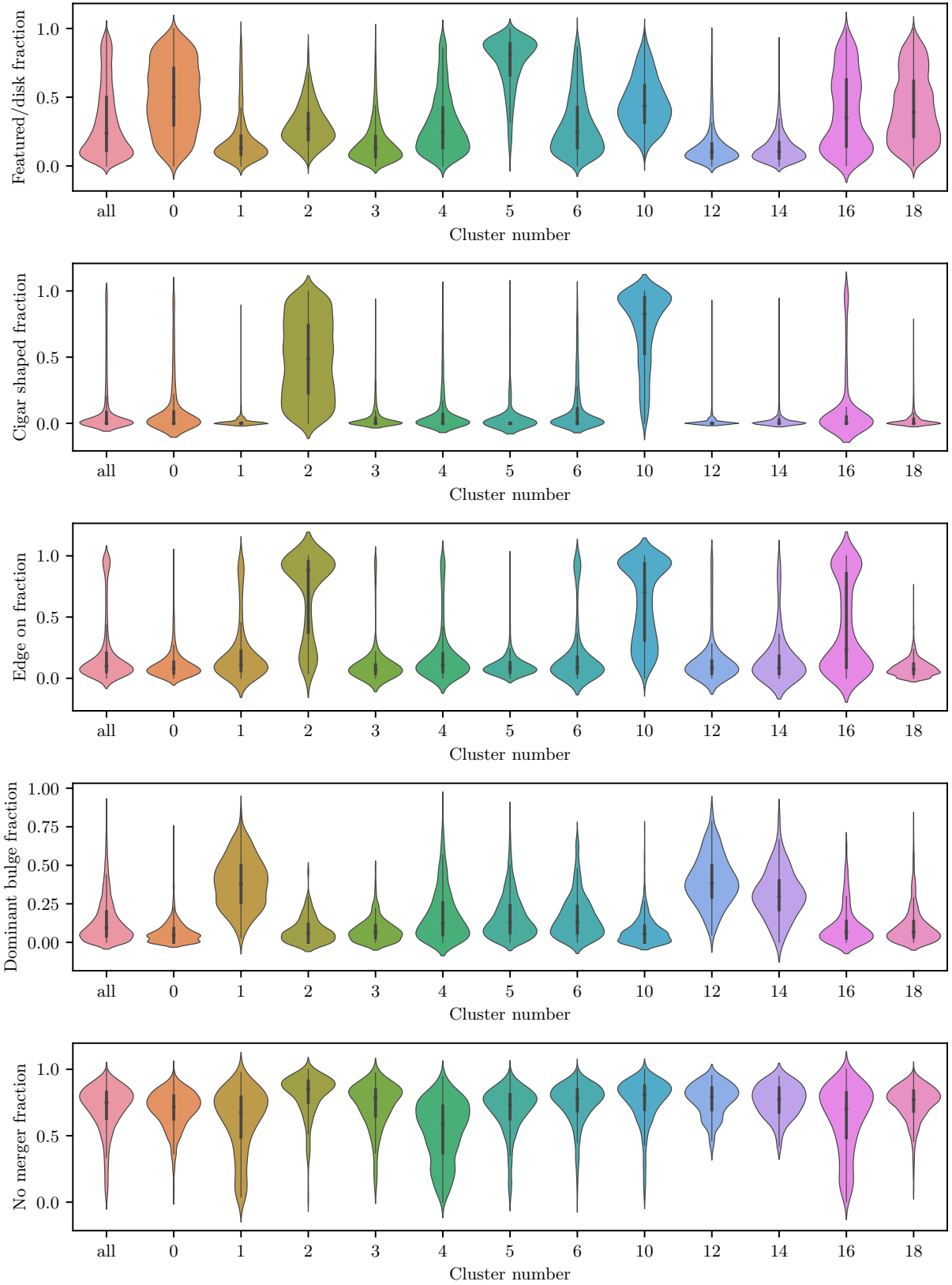


Figure 7. Vote fraction distributions for various Galaxy Zoo questions for each cluster (clusters of predominantly artefacts are not plotted). The global distribution is indicated with the “all” label. The distributions are represented as violin plots (using the package `SEABORN` (Waskom 2021)): a kernel density estimate of the distribution with lines representing the extrema, a box for the first and third quartiles and a point for the median. For clarity in distributions with long tails, the violins are set to equal width. These distributions can be used to investigate the types of galaxy morphology found in each cluster.

Cluster number	Description
0	Predominantly spiral galaxies
1	Mostly ellipticals and some spirals with prominent bulges
2	Edge-on disks and some cigar-shaped ellipticals
3	Predominantly ellipticals but does contain some spirals
4	A large mix of morphologies, including some apparent mergers and some artefacts
5	Almost entirely spiral galaxies
6	Mixed morphology, dominated by galaxies that have a (sometimes coincident) companion
7	Artefacts
8	Artefacts
9	Artefacts
10	Edge-on disks and some cigar-shaped ellipticals
11	Artefacts
12	Predominantly ellipticals
13	Artefacts
14	Predominantly ellipticals
15	Artefacts
16	A large mix of morphologies, including some apparent mergers and some artefacts
17	Artefacts
18	Predominantly spiral galaxies
19	Artefacts

Table 2. Qualitative summary of each of the clusters detected by applying a Bayesian Gaussian mixture model to the Galaxy Zoo DECaLS data.

may have merger candidates, although they will be mixed with other sources. Figure 5 shows that clusters 1, 4 and 16 both appear to have complex, multiple sources, with cluster 16 having more “zoomed out” examples.

Table 2 gives a qualitative description of the galaxies in each cluster, based on Figure 7 and Figures 4-6.

6.3 Cluster membership of evaluation subset

In Section 5.1 we introduced a “clean” and simple evaluation set of labelled objects, consisting of round ellipticals, spirals and edge-on spirals. We investigated which clusters these objects were assigned to:

- Round ellipticals - 77.2% found in clusters 12, 14, 3 and 1.
- Spirals - 79.3% found in clusters 5, 18 and 0.
- Edge-on spirals - 79.3% found in clusters 10, 2 and 6.

In all cases the majority of the sources were found in the first one or two clusters listed. These results broadly reflect the more qualitative conclusions drawn in Section 6.2.

How can this be useful? By simply inspecting a few objects in each cluster, we can apply labels to the clusters as above. This simple approach results in an overall accuracy of 77% for our evaluation subset. While this is clearly far below the performance of a supervised algorithm, it is impressively high for a fully unsupervised approach. This approach can be a highly efficient way to select and label samples for training downstream supervised learning algorithms, as well as being useful for removing artefacts and identifying unusual clusters of objects.

7 ANOMALY DETECTION

To further demonstrate the general utility of these self-supervised features, we applied anomaly detection to the dataset. Detecting rare and unusual objects in massive datasets is a key application of unsupervised learning. In order to compare with some ground truth labels and test performance, we focused on merger candidates as a specific type of anomalous object to search for. While it is completely possible to detect more rare types of sources with the same algorithm

and features, we did not have easy access to labels of such sources, and considered the merger example as a suitable anomaly detection demonstration.

7.1 Astronomy

We applied the ASTRONOMY framework (Lochner & Bassett 2021), with the alternative anomaly detection approach introduced in Walmley et al. (2022), which we found works well for this dataset. ASTRONOMY employs active learning to rapidly identify not just anomalies in data, but anomalies that are specifically of interest to the user. The key concept of ASTRONOMY is that “blind” anomaly detection, using machine learning, will usually detect a large number of sources which, while anomalous, are not of interest to a scientist. Thus, ASTRONOMY employs an interactive framework to obtain very few, strategic labels from a user in order to improve the detection algorithm. This is somewhat similar to recommendation engines used in popular music or video streaming services. In our case, uninteresting anomalies would include artefacts or galaxies with unusual morphologies, while anomalies of interest would be merger candidates. ASTRONOMY requires the user to score, on a scale of 0 to 5, examples of objects according to their “interestingness”. In machine learning nomenclature, the algorithm requests these labels from an “oracle”. Normally, this oracle would be a human expert who labels objects according to how interesting they are for the science interests of that expert. However, we had access to a set of ground truth labels from the citizen scientist volunteers to provide labels when requested by the algorithm. Although we have access to a large number of ground truth labels, only a subset of these were provided to the active learning algorithm.

We made use of the Galaxy Zoo decision tree question “*Is the galaxy merging or is there any sign of tidal debris?*”. This question has four possible answers: “Merging”, “Tidal debris”, “Both” or “Neither”. Visual inspection suggested that galaxies with a high voter fraction for “Tidal debris” are only mildly disturbed so we added the voter fractions for “Merging” and “Both” and took that number to be the probability that an image is a merging system. We scaled this probability to lie on the range of 0-5 and rounded to the nearest integer to simulate ASTRONOMY’s scoring mechanism. The key question

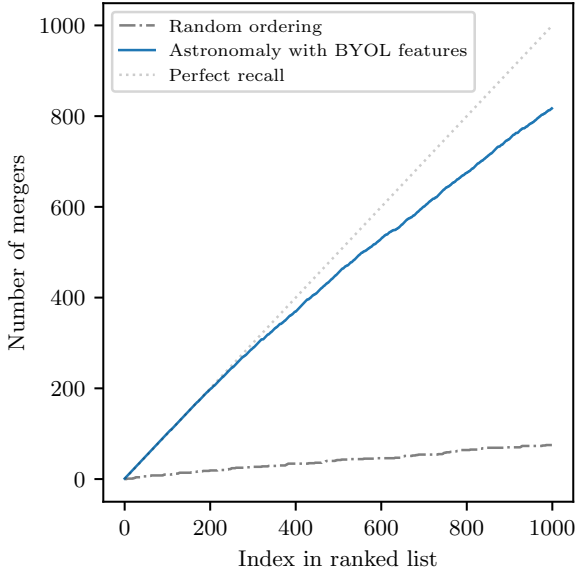


Figure 8. Number of mergers detected as a function of index in a list of sources ordered by anomaly score, after active learning is applied to 200 sources. The theoretical performance of a random order and perfect recall is shown for reference. *ASTRONOMY* is able to efficiently recover merger candidates without requiring significant labelling.

is, what threshold do we apply to decide if an image corresponds to a true positive merger? It seems overall voter confidence in this question was low since a high threshold (like 0.8) cuts out a large number of obvious merger candidates. We follow the methodology of Darg et al. (2010) and consider sources with a threshold of 0.4 to be very likely merger candidates. This will naturally not result in a very clean sample, but visual inspection suggests this cut is appropriate. We also ensure the voter fraction is at least 10 before considering a source a “true” merger. This results in 4990 mergers or 7% of the dataset considered as interesting anomalies.

We passed the features described in Section 4 after applying PCA to *ASTRONOMY*. The active learning approach of Walmsley et al. (2022) requires an initial sample of objects with labels. While Walmsley et al. (2022) used a random sample of galaxies to begin the process, we found that this introduces a large degree of randomness in the results, especially with small numbers of labels. Instead, in order to find a deterministic sample of galaxies that should broadly span the feature space, we sorted the features by their first principal component and selected an example from every tenth percentile (i.e. 10 objects equally spaced by index in the sorted list, not feature value). We labelled these with an integer score from 0 to 5, based on the merger probability.

This initial set of labels allowed us to proceed to the active learning step of the *ASTRONOMY* pipeline. The goal is to train a regression algorithm to learn, with as few examples as possible, to predict the “interestingness” score of every object in the dataset thus quickly finding the interesting anomalies. As in Walmsley et al. (2022), we use a Gaussian Process (GP) to perform the regression. A GP estimates a probability distribution of functions in order to predict the “interestingness” score at any given set of features. The space of possible functions is given by the kernel. We use a Matérn kernel, added to a white noise kernel to model intrinsic noise in the labelling, and allow the package *SCIKIT-LEARN* to automatically optimise kernel hyperparameters.

One of the most important advantages of a GP is that it calculates the uncertainty in its estimates, giving an indication of which regions of feature space are poorly constrained. This can be used in an acquisition function, which allows optimal selection of targets for the oracle to label in the next iteration that will improve the algorithm. We used exactly the same acquisition function as Walmsley et al. (2022), which is the maximum expected improvement. This function balances improving the score estimate across feature space by prioritising regions of high uncertainty and honing in on specific regions known to contain many high scoring objects. It has one tuning parameter, the trade-off η which we set to 0.5. This tends to prioritise known interesting regions over exploration, resulting in quickly finding mergers. We found that changing the η parameter did not strongly impact our results.

To perform our merger search, we labelled an initial 10 sources as described above and then trained the GP and labelled the top 10 unlabelled sources with the highest acquisition function. We repeated this process until 200 sources were labelled and then sorted the entire dataset according to estimated “interestingness” score. This corresponds to labelling just 0.3% of the data.

In general, *ASTRONOMY* does not classify sources as anomalous or not, rather sorting the list and allowing a user to decide how far down the list they are willing to explore in order to look for interesting sources. We can then consider the recall, in terms of number of interesting anomalies detected, as a function of index in the ranked list to determine the effectiveness of the anomaly detection algorithm, shown in Figure 8. The anomaly detection algorithm very efficiently recovers a large sample of mergers within the first few hundred sources with a high anomaly score. This excellent performance should obviously be taken with some caution as the threshold to be considered a merger is fairly low.

The two UMAP plots in Figure 9 demonstrate how the active learning score successfully maps the overdensity of mergers in feature space. While some mergers are buried among other, non-anomalous, sources, the majority are grouped together again highlighting that the self-supervised features effectively groups sources with visually similar morphology.

Figure 10 demonstrates that the majority of objects given a high score are indeed merger candidates. This figure attempts to demonstrate the active learning process by displaying the first five sources shown to the oracle each iteration, ordered by acquisition score (i.e. the five sources assigned the highest priority for labelling). After a few rounds querying some uninteresting objects, the algorithm quickly hones in on merger candidates which dominate the sources as quickly as the fifth query (40 sources labelled).

7.2 A similarity search for ring galaxies

Inspired by (Walmsley et al. 2022) and other recent works, we perform a similarity search for a particularly unusual type of source, in this case choosing a few candidate ring galaxies. These objects are truly rare and we could use *ASTRONOMY* to perform a dedicated search for them, however we have no ground truth labels to compare against so we instead opted to demonstrate the utility of the self-supervised features using a similarity search. We select two example ring galaxies and use a simple Euclidean search on the PCA-reduced feature space to find the eight nearest neighbours to each source.

Figure 11 and Figure 12 show the two selected sources and their eight nearest neighbours. It is clear that they share very similar morphology, indicating that these features can be useful for rapidly identifying samples of rare objects as soon as an initial example is discovered.

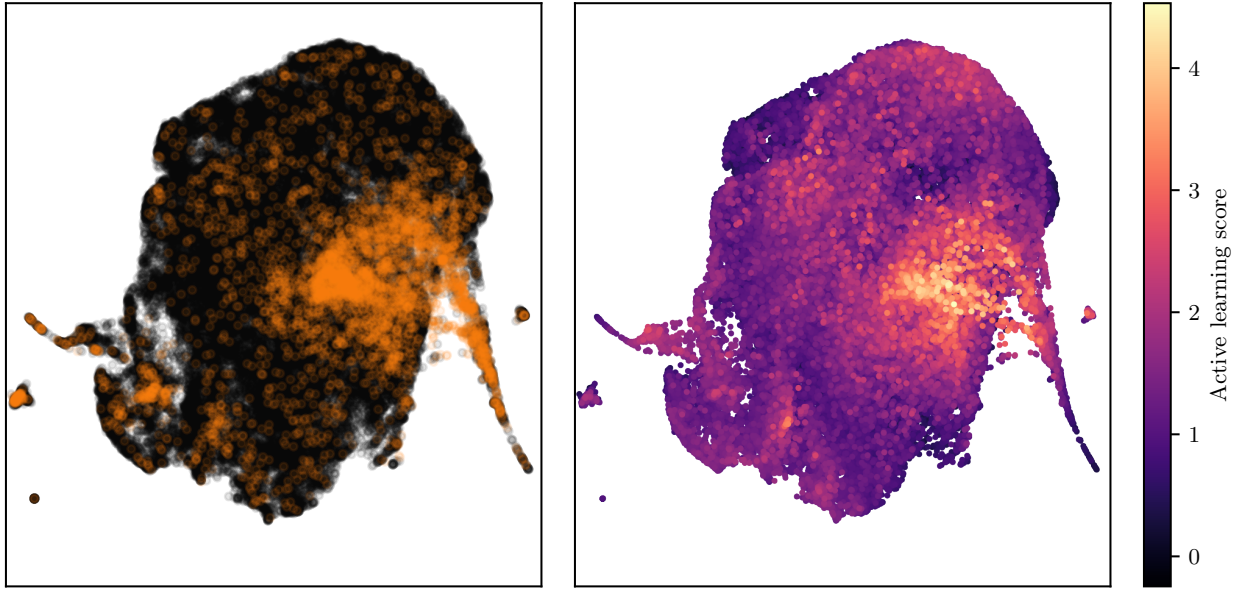


Figure 9. UMAP plots of the same Galaxy Zoo DECaLS feature space highlighting the “ground truth” mergers (left) and showing the anomaly score after applying active learning (right). It is clear that *ASTRONOMALY*, after training on just 200 examples, effectively prioritises the regions of feature space where mergers are likely to be found.

8 APPLICATION TO A RADIO DATASET

As a final application to test the general utility of self-supervised learning for feature extraction in astronomy, we turn to a completely different type of dataset and apply the exact same approach.

8.1 MiraBest data

We chose the radio image dataset MiraBest (Porter & Scaife 2023), a set of 1256 labelled radio images⁷ from the Karl G. Jansky Very Large Array⁸. Originally classified in Miraghaei & Best (2017), this sample of radio-loud active galactic nuclei consists of Fanaroff-Riley I and II sources, as well as some sources that appear to be hybrid between the two classes. The Fanaroff-Riley (FR) dichotomy, first proposed in Fanaroff & Riley (1974), is a morphological classification based on the distance of the brightest regions of the radio jets from the core. FRI galaxies become fainter towards the edge and tend to have a lower luminosity in general, while FR II galaxies are edge-brightened and more luminous. This is the most commonly used morphological classification in radio astronomy, although there is a high degree of variation in source morphology and many examples of sources that are challenging to classify. A random sample of FRI and FR II galaxies from the MiraBest dataset is shown in Figure 13.

We chose to apply our techniques to the MiraBest dataset for three reasons:

- (i) Radio images differ substantially from optical images, providing a good stress test for BYOL.
- (ii) There are very few labelled radio image datasets and MiraBest has the added advantage of distinguishing between confidently and unconfidently labelled sources. We could thus train BYOL on the full dataset but use only the confidently-labelled sources to evaluate.

- (iii) With new radio telescopes such as MeerKAT (Jonas & MeerKAT Team 2016), ASKAP (Hotan et al. 2021) and LOFAR (van Haarlem et al. 2013) pushing into new regimes of sensitivity, resolution and sky coverage, radio astronomy is a field where unsupervised learning is expected to prove extremely useful.

As the MiraBest sources were already cropped to some degree, we did not perform any resizing operation. We ran BYOL on this dataset using the exact same hyperparameters described in Section 4 except that we set the batch size to 32 (owing to the smaller dataset) and the number of epochs to 50, since we found that it took longer to produce useful representations. Even with the increased number of epochs, the small dataset size means we are able to train BYOL in just 11 minutes, using the same GPU mentioned in Section 4.1.

This dataset represents an interesting opportunity to test which is the best set of weights to initialise the network with. The idea is that so-called “foundation models”, already trained on large datasets, can then be easily fine-tuned using BYOL on smaller, different datasets for downstream tasks. We explore four scenarios for the weights initialisation:

- (1) Random weights
- (2) ImageNet trained weights
- (3) Galaxy Zoo DECaLS trained weights
- (4) Radio Galaxy Zoo trained weights

The last item on the list is derived from Slijepcevic et al. (2023) where BYOL was trained on a sample of non-public radio images. Fortunately, the authors made their trained model available and the architecture is similar to the model we used. We were able to use this model and fine-tune it to MiraBest. It is worth noting that this was also done in Slijepcevic et al. (2023) but there are some differences in approach, resulting in somewhat different accuracies achieved for the confident MiraBest sample.

⁷ Available at <https://zenodo.org/records/5588282>.

⁸ <https://science.nrao.edu/facilities/vla/>

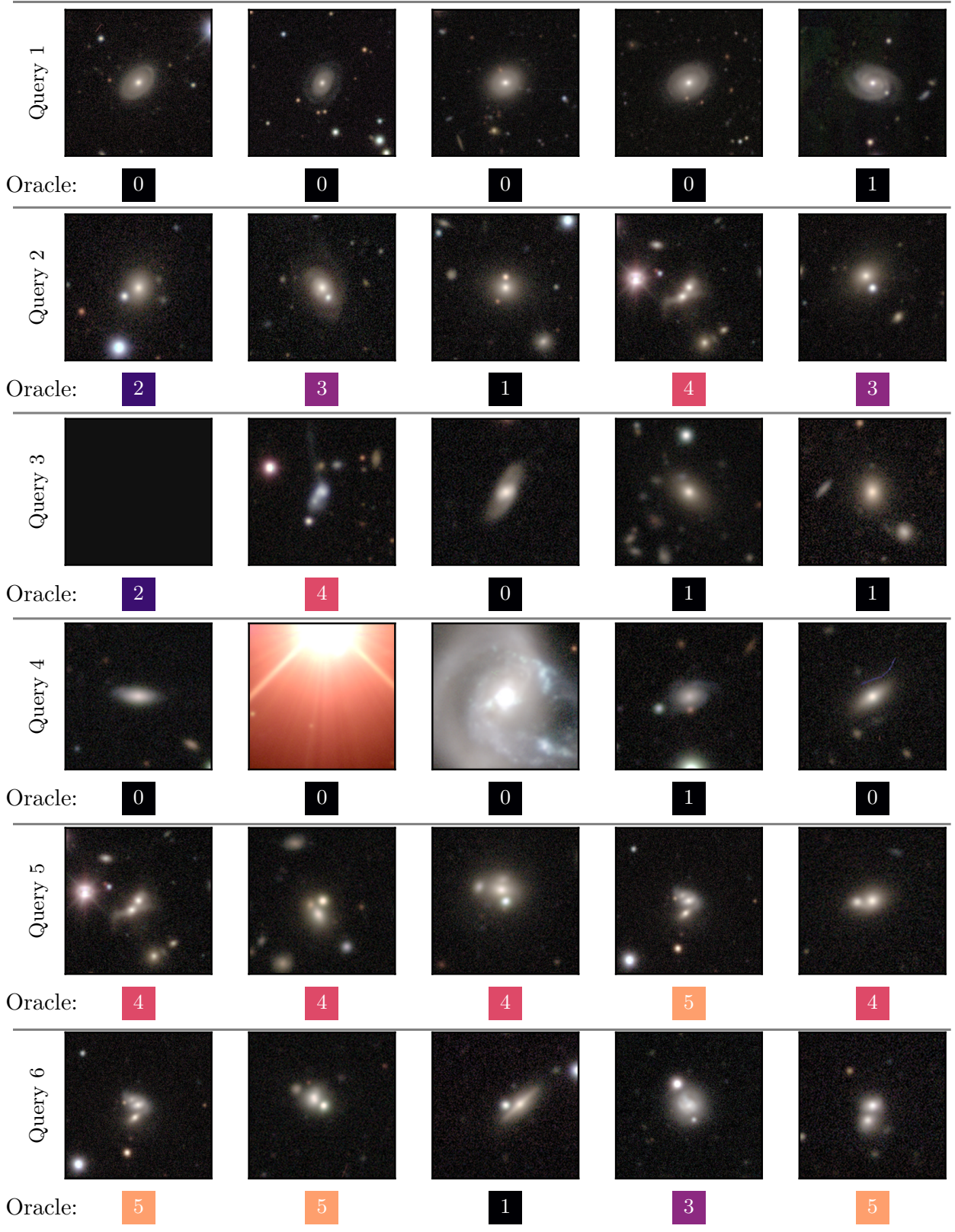


Figure 10. An illustration of the active learning approach used to detect anomalies (in this case merger candidates). Each iteration (query) consists of 10 examples being shown to the “oracle” after which the algorithm is retrained, ordered by acquisition score, and the next 10 objects are shown to the oracle. Only the top 5 examples for each query are shown here due to space considerations. The score the oracle gives (in this case, the labels are given from the citizen scientist votes) are shown in a box under each image. It can be seen that the algorithm quickly moves away from the more boring sources and hones in on merger candidates after seeing a handful of examples. Note that the blank image in query 3 is actually a completely black image in the Galaxy Zoo DECaLS dataset.

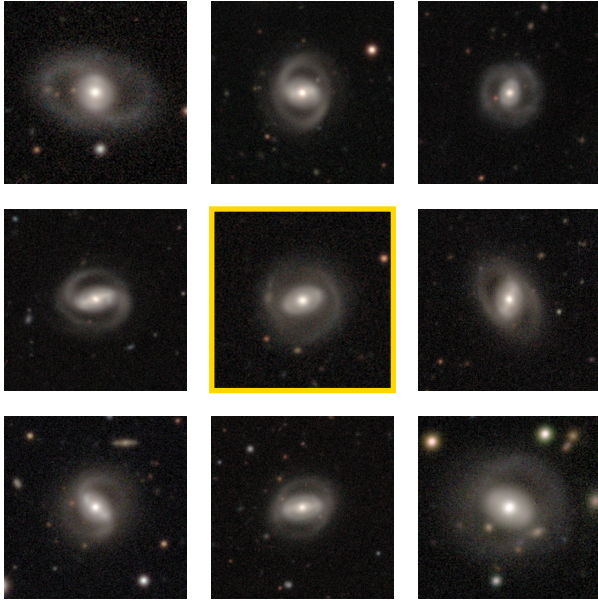


Figure 11. Similarity search for ring galaxies. The eight sources surrounding the central source are its eight nearest neighbours in feature space, according to the Euclidean distance.



Figure 12. Same as Figure 11, we highlight a specific ring galaxy (central source) and its eight nearest neighbours in feature space.

8.2 Evaluation

For each of the four scenarios, we trained a KNN on the confidently labelled data, used a 75%-25% training-test split and ran the classifier for 50 different random splits at each epoch. Figure 14 shows the accuracy as a function of epoch for each scenario. Firstly, it is clear that any of the three types of fine-tuning dramatically outperforms

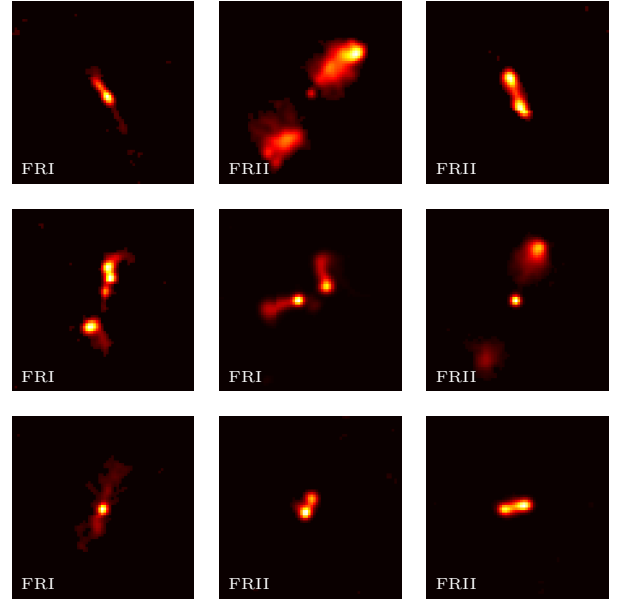


Figure 13. A random set of radio galaxies from the MiraBest training sample with the true label reported in the corner.

random weights, which tends instead towards a very poor representation in the limited number of epochs and with such a small training set. It is not surprising that fine-tuning from the Radio Galaxy Zoo network, trained using very similar data, outperforms all other options. The overall accuracy is comparable to that in Slijepcevic et al. (2023), if slightly lower because we are using KNN rather than a full CNN for the final classification step.

What is perhaps more interesting is that fine-tuning an ImageNet-trained network outperforms that of our Galaxy Zoo-trained network. This is counter-intuitive since radio galaxies are more similar to optical galaxies than terrestrial images of animals and objects. The reason for this performance difference could be because the ImageNet classification task involves of thousands of classes, forcing the network to learn very general representations (as was found in Walmsley et al. (2022)) or it may be simply due to the size of the training sets, with ImageNet being an order of magnitude larger than the Galaxy Zoo DECaLS sample we used. Either explanation bodes well for the general use of foundation models in astronomy as it suggests that a model trained on a completely different, but large, dataset can still be useful as a feature extractor if fine-tuned to the dataset it's being applied to.

This conclusion is further supported by examining the feature space of each of the four initialisations described above. Figure 15 shows the UMAP plot for each case for only the confident MiraBest sample, with FRI and FRII galaxies indicated with different markers. No separation between classes is seen when random weights are used, while the Radio Galaxy Zoo and ImageNet weights show fairly significant division between classes.

8.3 Clustering

Despite the small sample size, we managed to apply the same clustering approach as described in Section 6. We first applied PCA to each of the four sets of features with a threshold explained variance of 95%, resulting in reduced features of size 3, 31, 58 and 16 for the

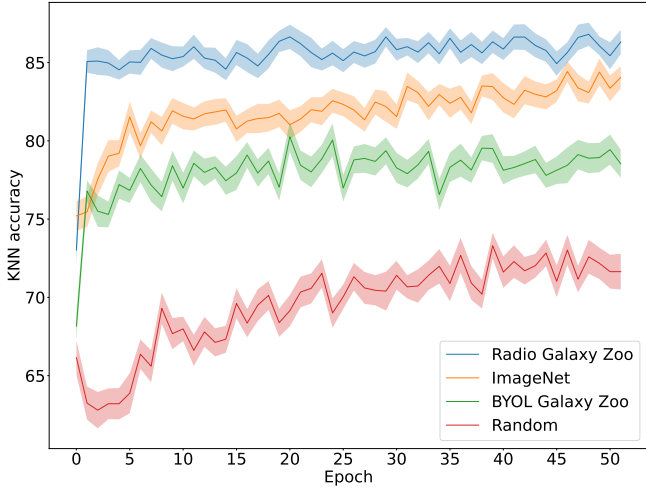


Figure 14. KNN accuracy as a function of epoch for the confidently-labelled MiraBest dataset for each of the four scenarios with different initialisation of the weights. It is clear that fine-tuning is superior to random-initialisation. Using a network trained on very similar data provides the highest performance but this can be almost matched by using a network trained a large dataset of terrestrial images (ImageNet).

random, ImageNet, Galaxy Zoo and Radio Galaxy Zoo weights respectively. We then applied a Bayesian Gaussian mixture model with up to 20 components to each set of reduced features. To simulate a real unsupervised learning application, we examine each cluster to check which is the dominant source in each. The cluster is then labelled as that source (i.e. if more than 50% of the objects in the cluster are FRI, all objects in the cluster are labelled FRI). While in this case we know the ground truth which makes the labelling easier, in a truly unlabelled dataset one would have to simply investigate a few samples and decide which is the dominant source for that cluster. By applying these labels, we can compute the overall accuracy of this pseudo-classifier, which is reported in Figure 15. Remarkably, we obtain almost as high accuracy as when we use a traditional KNN approach. This implies that a fully unsupervised approach, fine-tuning a foundation model and applying clustering, can at a minimum quickly produce potential training sets that can later be optimised through minimal human inspection and labelling.

9 CONCLUSIONS

Inspired by a rapid increase in size and complexity of astronomical datasets, we have explored an array of unsupervised learning methods for data exploration and scientific discovery. Deep learning has proven itself in the arena of supervised learning, but recently has begun to be used to obtain useful representations of high-dimensional data, such as images, without requiring expensive human-provided labels. We have shown that self-supervised learning, specifically the non-contrastive algorithm Bootstrap Your Own Latent (BYOL), is highly effective at feature extraction for astronomical images. We applied this algorithm to two quite different datasets: a sample of hundreds of thousands of optical images from Galaxy Zoo DECaLS and a relatively small set of radio galaxies from MiraBest. While the latent features perform well for a set of supervised learning tasks, the primary goal was to generate features suitable for unsupervised learning tasks, including clustering and anomaly detection.

As with any deep learning application, we found that preprocessing

choices are important. Our procedure to crop and resize each image, removing biases with respect to object size, inadvertently introduced artefacts in the data. However, we showed that these can be largely removed by applying an initial pretrained CNN as a feature extractor, visualising the space using the manifold embedding technique UMAP and cutting out an obvious large cluster of anomalies. This simple methodology could prove useful for very quickly identifying artefacts in other datasets as it requires no training at all. However, since the network was trained on a completely different dataset (ImageNet), it was not an appropriate feature extractor for more subtle distinctions between morphology.

By instead using the self-supervised learning algorithm BYOL, we were able to extract features for both the optical and radio dataset that performed well when combined with a k-nearest neighbours (KNN) algorithm to classify a subset of sources with known classes. While this approach is unlikely to compete with a purpose-built CNN when a large training set is available, it does demonstrate that BYOL is learning a useful representation of the data.

We used the same features for unsupervised learning applications, finding that a Bayesian Gaussian mixture model (BGMM) was able to successfully detect clusters of galaxies with similar morphologies for both datasets. For the Galaxy Zoo DECaLS dataset, we analysed the citizen scientist votes to determine the types of sources found in each cluster. While at times the algorithm places sources of different morphology in the same cluster (usually when confused by the presence of a coincident source or artefact), many clusters are relatively pure. For the MiraBest case, the accuracy of the fully unsupervised clustering method is close to that of a supervised KNN classifier.

This approach could be useful for quickly building initial training sets for subsequent supervised learning algorithms, which is currently a laborious process. While we did not explore this application here, one could imagine using the probability of a particular source belonging to a cluster (which is given by BGMM) to determine whether to include the source in the training set, or request an oracle (i.e. an expert or citizen scientist) to identify the source. A clustering analysis could also reveal unexpected groupings of sources in large, deep surveys.

For the Galaxy Zoo DECaLS dataset, we also applied the *ASTRONOMY* framework to detect anomalies. The only Galaxy Zoo decision tree category we had access to which could be considered anomalous was that of mergers, so we aimed to use anomaly detection to find merger candidates. We found that *ASTRONOMY* was able to use the BYOL-trained features to efficiently locate merger candidates, although this was using a relatively low cut on probability of being considered a merger (which was the same cut used in Darg et al. (2010)). We also showed how a similarity search can quickly identify candidate ring galaxies, another rare type of source. While unsupervised methods generally will not outperform a trained classifier, for cases where training data is sparse or the object in question is rare, the BYOL-derived features are clearly effective at locating objects of interest.

We found that fine-tuning the BYOL algorithm from the weights of a pretrained network far outperforms the more common approach of initialising the weights randomly. Interestingly, for the MiraBest data we found that ImageNet weights outperformed those from BYOL trained on Galaxy Zoo DECaLS, despite the optical dataset being far more similar to the radio than the terrestrial one. This could be due to the much larger dataset when performing the initial training or the fact that the network in question was trained to classify a large number of diverse classes. This question could be answered by initialising the weights from a network trained with BYOL or another self-supervised learning method, rather than supervised learning, to

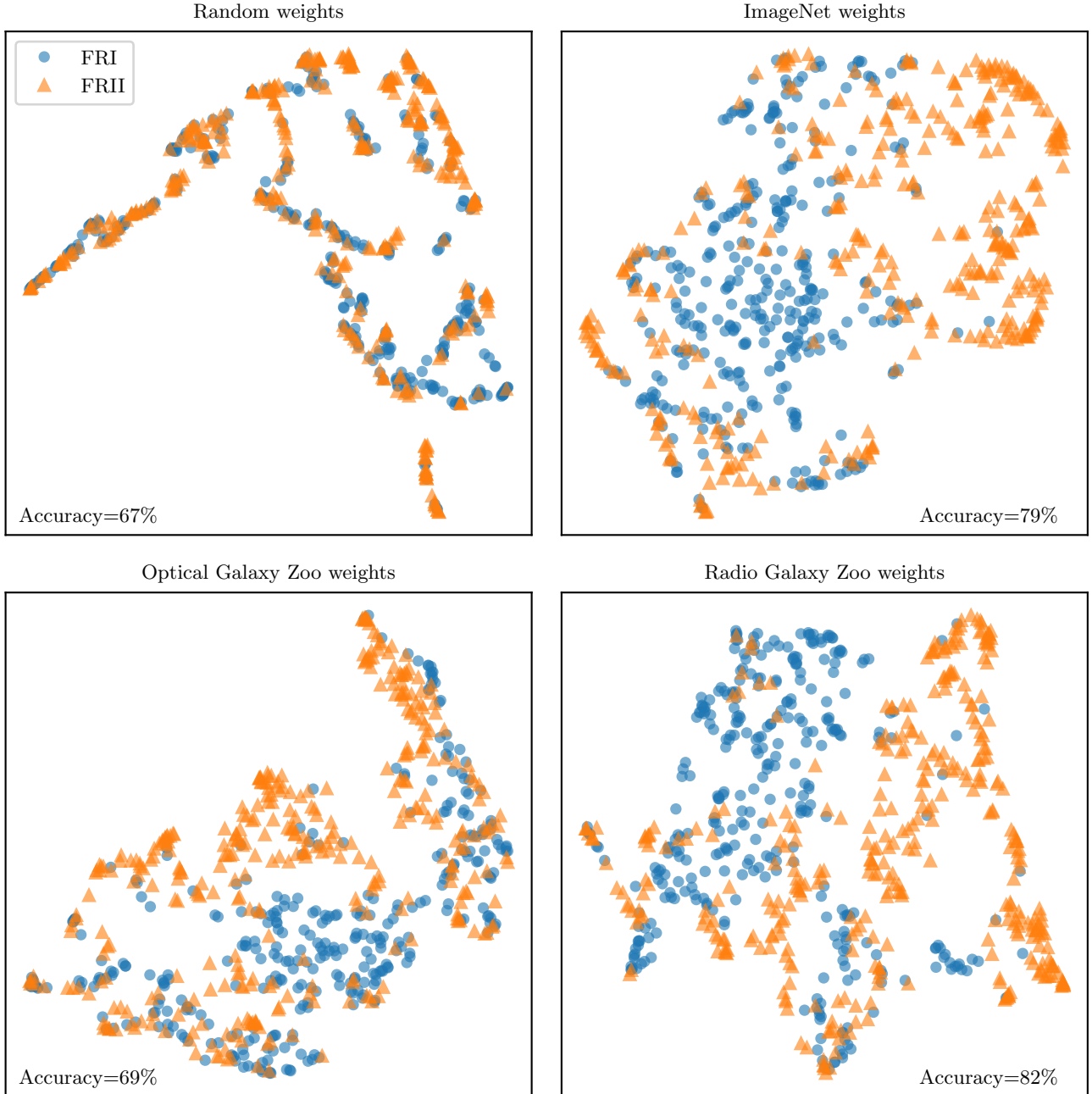


Figure 15. UMAP plots for four different sets of initial weights: random (top left), ImageNet (top right), our Galaxy Zoo-trained BYOL (bottom left) and the BYOL trained on Radio Galaxy Zoo from [Slijepcevic et al. \(2023\)](#) (bottom right). The features are shown for the confident MiraBest sample only and FRI and FRII galaxies are indicated with different symbols. When clustering is applied, if we assign an entire cluster with the same class as the majority source in that cluster, we obtain the accuracy indicated in each figure. This accuracy is close to that of the supervised approach shown in [Figure 14](#), indicating that BYOL successfully learns features useful for both clustering and supervised classification. Finally, both the accuracy and the visual appearance of the UMAP plots seem to suggest that a large training set is an important factor when fine-tuning a pretrained network, as the ImageNet weights outperform the optical Galaxy Zoo weights despite the fact that they are derived from a dataset less similar to MiraBest.

identify which approach produces the most useful starting weights. Less surprisingly, we found a network trained (using BYOL) on a large set of radio galaxies outperformed all others when fine-tuned on MiraBest. This bodes well for the idea of providing foundation models, trained on large datasets, for astronomical data which can

then be fine-tuned to any specific dataset and used for downstream tasks.

The key challenge in applying unsupervised methods to image data is usually feature extraction. This work demonstrates that this challenge can be overcome by leveraging self-supervised methods to extract meaningful representations of the data. These representations

enable automated clustering, which in turn allows for a rapid removal of artefacts, a faster route to labelled training sets and the potential for discovering new patterns in the data. The same representations can also be used to find rare sources and even discover new classes of objects with minimal human intervention.

ACKNOWLEDGEMENTS

ML and KM acknowledge support from the South African Radio Astronomy Observatory and the National Research Foundation (NRF) towards this research. Opinions expressed and conclusions arrived at, are those of the authors and are not necessarily to be attributed to the NRF.

Author contribution statements: KM lead the research and development, including conceptualisation of many of the key ideas, and produced an early draft of the paper. ML supervised the project, performed the analysis in Section 6.2, Section 7 and Section 8.3 and wrote the majority of the paper.

This research made use of the python programming language and the following open source packages: Numpy, SciPy (Jones et al. 2001), Matplotlib (Hunter 2007), Seaborn (Waskom 2021), scikit-learn (Pedregosa et al. 2011), Pandas (McKinney 2010), Astropy (The Astropy Collaboration et al. 2013, 2018), umap-learn (Sainburg et al. 2021), PyTorch (Paszke et al. 2019) and BYOL-PyTorch (Chen & He 2020). The authors also acknowledge the surprising helpfulness of ChatGPT⁹ in coming up with ideas for the title based on the (human-written) abstract. It was not used for any other aspect of the paper.

We acknowledge the use of the ilifu cloud computing facility – www.ilifu.ac.za, a partnership between the University of Cape Town, the University of the Western Cape, the University of Stellenbosch, Sol Plaatje University and the Cape Peninsula University of Technology. The Ilifu facility is supported by contributions from the Inter-University Institute for Data Intensive Astronomy (IDIA – a partnership between the University of Cape Town, the University of Pretoria and the University of the Western Cape, the Computational Biology division at UCT and the Data Intensive Research Initiative of South Africa (DIRISA).

This publication uses data generated via the Zooniverse.org platform, development of which is funded by generous support, including a Global Impact Award from Google, and by a grant from the Alfred P. Sloan Foundation.

The Legacy Surveys consist of three individual and complementary projects: the Dark Energy Camera Legacy Survey (DECaLS; Proposal ID #2014B-0404; PIs: David Schlegel and Arjun Dey), the Beijing-Arizona Sky Survey (BASS; NOAO Prop. ID #2015A-0801; PIs: Zhou Xu and Xiaohui Fan), and the Mayall z -band Legacy Survey (MzLS; Prop. ID #2016A-0453; PI: Arjun Dey). DECaLS, BASS and MzLS together include data obtained, respectively, at the Blanco telescope, Cerro Tololo Inter-American Observatory, NSF’s NOIRLab; the Bok telescope, Steward Observatory, University of Arizona; and the Mayall telescope, Kitt Peak National Observatory, NOIRLab. Pipeline processing and analyses of the data were supported by NOIRLab and the Lawrence Berkeley National Laboratory (LBNL). The Legacy Surveys project is honoured to be permitted to conduct astronomical research on Iolkam Du’ag (Kitt Peak), a mountain with particular significance to the Tohono O’odham Nation. NOIRLab is operated by the Association of Universities for

Research in Astronomy (AURA) under a cooperative agreement with the National Science Foundation. LBNL is managed by the Regents of the University of California under contract to the U.S. Department of Energy. This project used data obtained with the Dark Energy Camera (DECam), which was constructed by the Dark Energy Survey (DES) collaboration. Funding for the DES Projects has been provided by the U.S. Department of Energy, the U.S. National Science Foundation, the Ministry of Science and Education of Spain, the Science and Technology Facilities Council of the United Kingdom, the Higher Education Funding Council for England, the National Center for Supercomputing Applications at the University of Illinois at Urbana-Champaign, the Kavli Institute of Cosmological Physics at the University of Chicago, Center for Cosmology and Astro-Particle Physics at the Ohio State University, the Mitchell Institute for Fundamental Physics and Astronomy at Texas A&M University, Financiadora de Estudos e Projetos, Fundacao Carlos Chagas Filho de Amparo, Financiadora de Estudos e Projetos, Fundacao Carlos Chagas Filho de Amparo a Pesquisa do Estado do Rio de Janeiro, Conselho Nacional de Desenvolvimento Cientifico e Tecnologico and the Ministerio da Ciencia, Tecnologia e Inovacao, the Deutsche Forschungsgemeinschaft and the Collaborating Institutions in the Dark Energy Survey. The Collaborating Institutions are Argonne National Laboratory, the University of California at Santa Cruz, the University of Cambridge, Centro de Investigaciones Energeticas, Medioambientales y Tecnologicas-Madrid, the University of Chicago, University College London, the DES-Brazil Consortium, the University of Edinburgh, the Eidgenossische Technische Hochschule (ETH) Zurich, Fermi National Accelerator Laboratory, the University of Illinois at Urbana-Champaign, the Institut de Ciencies de l’Espai (IEEC/CSIC), the Institut de Fisica d’Altes Energies, Lawrence Berkeley National Laboratory, the Ludwig Maximilians Universitat Munchen and the associated Excellence Cluster Universe, the University of Michigan, NSF’s NOIRLab, the University of Nottingham, the Ohio State University, the University of Pennsylvania, the University of Portsmouth, SLAC National Accelerator Laboratory, Stanford University, the University of Sussex, and Texas A&M University. BASS is a key project of the Telescope Access Program (TAP), which has been funded by the National Astronomical Observatories of China, the Chinese Academy of Sciences (the Strategic Priority Research Program “The Emergence of Cosmological Structures” Grant # XDB09000000), and the Special Fund for Astronomy from the Ministry of Finance. The BASS is also supported by the External Cooperation Program of Chinese Academy of Sciences (Grant # 114A11KYSB20160057), and Chinese National Natural Science Foundation (Grant # 12120101003, # 11433005). The Legacy Survey team makes use of data products from the Near-Earth Object Wide-field Infrared Survey Explorer (NEOWISE), which is a project of the Jet Propulsion Laboratory/California Institute of Technology. NEOWISE is funded by the National Aeronautics and Space Administration. The Legacy Surveys imaging of the DESI footprint is supported by the Director, Office of Science, Office of High Energy Physics of the U.S. Department of Energy under Contract No. DE-AC02-05CH1123, by the National Energy Research Scientific Computing Center, a DOE Office of Science User Facility under the same contract; and by the U.S. National Science Foundation, Division of Astronomical Sciences under Contract No. AST-0950945 to NOAO.

⁹ <https://chat.openai.com/>

DATA AVAILABILITY

The data used in this paper are publicly available at <https://zenodo.org/record/4573248> for the Galaxy Zoo DECaLS data and <https://zenodo.org/records/5588282> for the MiraBest data.

REFERENCES

- Attias H., 1999, *Advances in neural information processing systems*, 12
- Bradski G., 2000, *Dr. Dobb's Journal of Software Tools*
- Chen X., He K., 2020, *Exploring Simple Siamese Representation Learning* ([arXiv:2011.10566](https://arxiv.org/abs/2011.10566))
- Chen T., Kornblith S., Norouzi M., Hinton G., 2020, *A Simple Framework for Contrastive Learning of Visual Representations*, doi:10.48550/ARXIV.2002.05709, <https://arxiv.org/abs/2002.05709>
- Cheng T.-Y., Huertas-Company M., Conselice C. J., Aragón-Salamanca A., Robertson B. E., Ramachandra N., 2021, *MNRAS*, **503**, 4446
- Cover T., Hart P., 1967, *IEEE Transactions on Information Theory*, 13, 21
- Darg D. W., et al., 2010, *Monthly Notices of the Royal Astronomical Society*, **401**, 1043
- Dey A., et al., 2019, *The Astronomical Journal*, **157**, 168
- Domínguez Sánchez H., Huertas-Company M., Bernardi M., Tuccillo D., Fischer J. L., 2018, *MNRAS*, **476**, 3661
- Etsebeth V., Lochner M., Walmsley M., Grespan M., 2023, *Astronomy at Scale: Searching for Anomalies Amongst 4 Million Galaxies* ([arXiv:2309.08660](https://arxiv.org/abs/2309.08660))
- Fanaroff B. L., Riley J. M., 1974, *MNRAS*, **167**, 31P
- Fielding E., Nyirenda C. N., Vaccari M., 2022, in *2022 International Conference on Electrical*. p. 1 ([arXiv:2206.06165](https://arxiv.org/abs/2206.06165)), doi:10.1109/ICECET55527.2022.9872611
- Fix E., Hodges J., 1951, *Discriminatory Analysis: Nonparametric Discrimination: Consistency Properties*. USAF School of Aviation Medicine, <https://books.google.co.za/books?id=4XwytAEACAAJ>
- Grill J.-B., et al., 2020, *Advances in neural information processing systems*, **33**, 21271
- Guérin J., Thiery S., Nyiri E., Gibaru O., Boots B., 2021, *Neurocomputing*, **423**, 551
- Gupta N., Huynh M., Norris R. P., Wang X. R., Hopkins A. M., Andernach H., Koribalski B. S., Galvin T. J., 2022, *Publ. Astron. Soc. Australia*, **39**, e051
- Hayat M. A., Stein G., Harrington P., Lukić Z., Mustafa M., 2021, *The Astrophysical Journal Letters*, **911**, L33
- He K., Zhang X., Ren S., Sun J., 2016, in *2016 IEEE Conference on Computer Vision and Pattern Recognition (CVPR)*. pp 770–778, doi:10.1109/CVPR.2016.90
- Hotan A. W., et al., 2021, *Publ. Astron. Soc. Australia*, **38**, e009
- Hotelling H., 1933, *Journal of Educational Psychology*, **24**, 417
- Huertas-Company M., Sarmiento R., Knapen J., 2023, *A brief review of contrastive learning applied to astrophysics* ([arXiv:2306.05528](https://arxiv.org/abs/2306.05528))
- Hunter J. D., 2007, *Computing in Science and Engineering*, **9**, 99
- Jonas J., MeerKAT Team 2016, in *MeerKAT Science: On the Pathway to the SKA*. p. 1
- Jones E., Oliphant T., Pearu P., Others 2001, *SciPy: Open Source Scientific Tools for Python*, <http://www.scipy.org/>
- Lahav O., Naim A., Sodr  L. J., Storrie-Lombardi M. C., 1996, *MNRAS*, **283**, 207
- LeCun Y., Bengio Y., Hinton G., 2015, *Nature*, **521**, 436
- Lintott C. J., et al., 2008, *Monthly Notices of the Royal Astronomical Society*, **389**, 1179
- Lochner M., Bassett B. A., 2021, *Astronomy and Computing*, **36**, 100481
- Lochner M., Rudnick L., Heywood I., Knowles K., Shabala S. S., 2023, *Monthly Notices of the Royal Astronomical Society*, **520**, 1439
- McInnes L., Healy J., Melville J., 2018, *arXiv e-prints*, p. [arXiv:1802.03426](https://arxiv.org/abs/1802.03426)
- McKinney W., 2010, *Data Structures for Statistical Computing in Python*, <http://conference.scipy.org/proceedings/scipy2010/mckinney.html>
- Miraghaei H., Best P. N., 2017, *MNRAS*, **466**, 4346
- Naim A., Ratnatunga K. U., Griffiths R. E., 1997, *arXiv e-prints*, pp astro-ph/9704012
- Paszke A., et al., 2019, *arXiv e-prints*, p. [arXiv:1912.01703](https://arxiv.org/abs/1912.01703)
- Pearson K., 1901, *The London, Edinburgh, and Dublin Philosophical Magazine and Journal of Science*, **2**, 559
- Pedregosa F., et al., 2011, *Journal of Machine Learning Research*, **12**, 2825
- Polsterer K. L., Gieseke F., Doser B., 2019, *PINK: Parallelized rotation and flipping INvariant Kohonen maps* (ascl:1910.001)
- Porter F. A. M., Scaife A. M. M., 2023, *RAS Techniques and Instruments*, **2**, 293
- Ralph N. O., et al., 2019, *PASP*, **131**, 108011
- Russakovsky O., et al., 2014, *ImageNet Large Scale Visual Recognition Challenge*, doi:10.48550/ARXIV.1409.0575, <https://arxiv.org/abs/1409.0575>
- Sainburg T., McInnes L., Gentner T. Q., 2021, *Neural Computation*, **33**, 2881
- Sarmiento R., Huertas-Company M., Knapen J. H., Sánchez S. F., Domínguez Sánchez H., Drory N., Falc n-Barroso J., 2021, *ApJ*, **921**, 177
- Schawinski K., et al., 2009, *Proceedings of the International Astronomical Union*, **5**, 438
- Simmons B. D., et al., 2014, *Monthly Notices of the Royal Astronomical Society*, **445**, 3466
- Slijepcevic I. V., Scaife A. M. M., Walmsley M., Bowles M., Wong O. I., Shabala S. S., White S. V., 2023, *Radio Galaxy Zoo: Building a multi-purpose foundation model for radio astronomy with self-supervised learning* ([arXiv:2305.16127](https://arxiv.org/abs/2305.16127))
- Spindler A., Geach J. E., Smith M. J., 2021, *MNRAS*, **502**, 985
- Stein G., Harrington P., Blaum J., Medan T., Lukic Z., 2021, *arXiv e-prints*, p. [arXiv:2110.13151](https://arxiv.org/abs/2110.13151)
- Stein G., Blaum J., Harrington P., Medan T., Lukić Z., 2022, *ApJ*, **932**, 107
- The Astropy Collaboration et al., 2013, *A&A*, **558**, A33
- The Astropy Collaboration et al., 2018, *The Astronomical Journal*, **156**, 123
- The Astropy Collaboration et al., 2022, *The Astrophysical Journal*, **935**, 167
- Tian Y., Chen X., Ganguli S., 2021, *arXiv e-prints*, p. [arXiv:2102.06810](https://arxiv.org/abs/2102.06810)
- Vafaei Sadr A., Bassett B. A., Sekyi E., 2022, *arXiv e-prints*, p. [arXiv:2210.16334](https://arxiv.org/abs/2210.16334)
- Walmsley M., et al., 2020a, *Galaxy Zoo DECaLS: Detailed Visual Morphology Measurements from Volunteers and Deep Learning for 314,000 Galaxies*, doi:10.5281/zenodo.4196267, <https://doi.org/10.5281/zenodo.4196267>
- Walmsley M., et al., 2020b, *Galaxy Zoo DECaLS: Detailed Visual Morphology Measurements from Volunteers and Deep Learning for 314,000 Galaxies*, doi:10.5281/zenodo.4573248, <https://doi.org/10.5281/zenodo.4573248>
- Walmsley M., et al., 2022, *Monthly Notices of the Royal Astronomical Society*, **513**, 1581
- Waskom M. L., 2021, *Journal of Open Source Software*, **6**, 3021
- Webb S., et al., 2020, *Monthly Notices of the Royal Astronomical Society*, **498**, 3077–3094
- Wei S., Li Y., Lu W., Li N., Liang B., Dai W., Zhang Z., 2022, *PASP*, **134**, 114508
- Yang H.-F., et al., 2023, *Research in Astronomy and Astrophysics*, **23**, 055006
- Zhou C., Gu Y., Fang G., Lin Z., 2022, *AJ*, **163**, 86
- d'Abrusco R., Longo G., Paolillo M., de Filippis E., Brescia M., Staiano A., Tagliaferri R., 2007, *arXiv e-prints*, pp astro-ph/0701137
- van Haarlem M. P., et al., 2013, *A&A*, **556**, A2
- van der Maaten L., Hinton G., 2008, *Journal of Machine Learning Research*, **9**, 2579

This paper has been typeset from a $\mathrm{\TeX}/\mathrm{\LaTeX}$ file prepared by the author.